Validation of the 1,4-Butanediol thermoplastic polyurethane (b-TPUe) as a novel material for 3D bioprinting applications

Carlos Chocarro-Wrona[1,2,3,4], Juan de Vicente[4 5], Cristina Antich[1,2,3,4], Gema Jiménez[1,2,4], Daniel Martínez-Moreno[1,2,3,4], Esmeralda Carrillo[1,2,3,4], Elvira Montañez[6,7], Patricia Gálvez-Martín[8,9], Macarena Perán[1,2,4,10], Elena López-Ruiz[1,2,4,10], Juan A. Marchal[1,2,3,4 *].*

1. Biosanitary Research Institute of Granada (ibs.GRANADA), University Hospitals of Granada-University of Granada, Granada, Spain.
2. Biopathology and Regenerative Medicine Institute (IBIMER), Centre for Biomedical Research (CIBM), University of Granada, Granada, Spain.
3. Department of Human Anatomy and Embryology, Faculty of Medicine, University of Granada, Granada, Spain.
4. Excellence Research Unit "Modeling Nature" (MNat), University of Granada, Granada, Spain.
5. Department of Applied Physics, Faculty of Sciences, University of Granada, Granada, Spain.

6. Biomedical Research Institute of Málaga (IBIMA), Málaga.

7. Department of Orthopedic Surgery and Traumatology, Virgen de la Victoria University Hospital, 29010 Málaga, Spain.

8. Department of Pharmacy and Pharmaceutical Technology, School of Pharmacy, University of Granada, Granada, Spain.

9. Advanced Therapies Area, Bioibérica S.A.U., Barcelona, Spain.

10. Department of Health Sciences, University of Jaén, Jaén, Spain.

* Corresponding authors.

Contact information:

Corresponding Authors

* Prof. Juan Antonio Marchal, MD, PhD: e-mail: jmarchal@ugr.es.

* Elena López-Ruiz; e-mail: elop@ugr.es

Abstract

Background

Tissue engineering (TE) seeks to fabricate implants that mimic the mechanical strength, structure, and composition of native tissues. Cartilage TE requires the development of functional personalized implants with cartilage-like mechanical properties capable of sustaining high load-bearing environments to integrate into the surrounding tissue of the cartilage defect.

Objective

In this study we evaluated the novel 1,4-Butanediol thermoplastic polyurethane elastomer (b-TPUe) derivative filament as a 3D bioprinting material with application in cartilage TE.

Methods

The mechanical behaviour of b-TPUe in terms of friction and elasticity were examined and compared with human articular cartilage, PCL, and PLA. Moreover, infrapatellar fat pad-derived human mesenchymal stem cells (MSCs) were bioprinted together with scaffolds. *In vitro* cytotoxicity, proliferative potential, cell viability, and chondrogenic differentiation were analysed by Alamar blue assay, SEM, confocal microscopy, and RT-qPCR. Moreover, *in vivo* biocompatibility and host integration were analysed.

Results

b-TPUe demonstrated a much closer compression and shear behaviour to native cartilage than PCL and PLA, as well as closer tribological properties to cartilage. Moreover, b-TPUe bioprinted scaffolds were able to maintain proper proliferative potential, cell viability, and supported MSCs chondrogenesis. Finally, *in vivo* studies revealed no toxic effects 21 days after scaffolds implantation, extracellular matrix (ECM) deposition and integration within the surrounding tissue.

Conclusions

This is the first study that validates the biocompatibility of b-TPUe for 3D bioprinting. Our findings indicate that this biomaterial can be exploited for the automated biofabrication of artificial tissues with tailorable mechanical properties including the great potential for cartilage TE applications.

Keywords: 3D bioprinting, 1,4-Butanediol thermoplastic polyurethane, elastomer, tissue

engineering, MSCs.

1. Introduction

In the last few years the 3D bioprinting technology has shown promising results in the biofabrication of artificial tissues for tissue engineering (TE) applications (1). This emerging technology uses computer-aided design (CAD) and computer-aided manufacturing (CAM) techniques, which in combination with the layer-by-layer fabrication nature of 3D printing, allows to create structures with different geometries while controlling the spatial distribution of cells, biomaterials, and growth factors (2,3). Furthermore, 3D bioprinting brings advantages to the clinical field such as shorter fabrication time, higher precision than conventional TE techniques, and tailored production (4).

Among 3D bioprinting techniques, extrusion-based is the most extended as it offers the possibility to print a wide variety of biomaterial viscosities and is the most adaptable technology to be transferred to the clinical field (5,6). Additionally, there are several commercially available extrusion-based bioprinters, and they can also be adapted for testing novel biomaterials. Although this approach holds great promises for TE and regenerative medicine, as an emerging technology it also entails some bottlenecks. One of the main challenges is the restricted accessibility of materials necessary to produce constructs that can properly mimic the native tissue properties. The most common type of material used for this purpose are hydrogels, since they can offer a suitable 3D microenvironment that mimics the extracellular matrix (ECM) of natural tissues, promoting cell attachment and proliferation (7). However, hydrogel scaffolds usually lack mechanical strength and structural integrity, therefore, their mechanical properties need to be tuned or combined with synthetic stiffer biomaterials to enhance its mechanical properties (8).

Several synthetic materials such as PLA (9–11), PCL (12–15) or polylactic-co-glycolic acid (PLGA) (16–19) have been used to generate bioprinted scaffolds for TE applications. However,

these materials do not easily achieve to mimic the native tissue mechanical characteristics. The stiffness of porous scaffolds produced using rigid biomaterials, such as PLA (20), are in the MPa magnitude order comparable to those found in hard tissues such as porous bone (21). Therefore, significant efforts are being made for engineering flexible tissues that suffer mechanical loading such as ligaments, tendons, cartilage, blood vessels, skin, or muscles (22).

In this sense, cartilage, as an avascular and stratified tissue, presents a limited capacity of repair, therefore, a severe damage will often require surgical intervention. However, the clinical surgical treatments such as ACI or MACI, which use a bilayer type I/III collagen membrane, lack long-term effectiveness (23–25). Mosaicplasty, a treatment for focal chondral lesions, shows results that are relatively acceptable for the first 2 years but develops a sudden failure rate (approximatively 55%) over the successive 2 years (26). Currently, the strategies for cartilage repair are concentrated on the creation of a complex material that biologically mimics the native tissue and get close to its biomechanical properties. Hence, many biomaterials, such as fibrin, silk, hyaluronic acid, chitosan, PLA or PCL (27) are being used to create scaffolds for cartilage tissue engineering, but, on one hand, natural-based materials do not show enough integrity, and on the other hand, synthetic-based materials do not have similar mechanical properties to cartilage such as friction and elasticity which limits their effectiveness and integration in the injury (28,29).

Polyurethane elastomers are a type of adaptable synthetic materials broadly applied to biomedical purposes because of their biocompatibility and good mechanical properties (30–32). Recently, a novel elastic 3D printing filament consistent of a 1,4-Butanediol Thermoplastic Polyurethane (b-TPUe) derivative shows a combination of mechanical properties that makes it a promising candidate for TE (33).

In this study we evaluate, for the first time, the potential use of b-TPUe filament as a new 3D bioprinting material for biomedical applications. We carried out a rheological characterization to analyse their mechanical properties (in shear and compression) and a tribological study to evaluate the frictional behaviour in synovial fluid-lubricated b-TPUe-cartilage tribopairs. Moreover, we compared *in vitro* and *in vivo* the biocompatibility of b-TPUe 3D printed scaffolds versus PCL and showed the potential application of this material for cartilage TE. Finally, we described the induced chondrogenic differentiation of MSCs isolated from infrapatellar fat pad when cultured in 3D bioprinted b-TPUe scaffolds. In conclusion we present a novel use of b-TPUe filament with potential to support the development of cartilage-like phenotype as a promising TE biomaterial.

2. Results

2.1. Fabrication of scaffolds

3D b-TPUe scaffolds were designed with a regular geometry and structure to enable an adequate cell bioprinting **(Figure 1A)** and successfully fabricated with the desired shape and dimensions, like the CAD model **(Figure 1B)**. Scanning electron microscope (SEM) images **(Figure 1C and 1D)** show the obtained scaffold pores and filament surfaces and demonstrate that the thickness of the fibres of the b-TPUe printed scaffolds (200 - 400 μm) is maintained during the fabrication process **(Figure 1E-J)**. As can be clearly seen, the pores are large, ranging from 500 to 700 μm **(Figure 1C and 1D)** and have a regular structure, uniformly distributed, and interconnected.

2.2. Frictional test

The frictional behaviour of the different plastics used in this work is exemplified in **figure 2A** and **2B**. For this, plastic-cartilage point contacts were lubricated by synovial fluid and data are plotted in terms of a Stribeck curve, where friction coefficient is represented as a function of the sliding speed for a constant normal load of 1 N. Only for b-TPUe, the contact operates in the full film lubricated regime as demonstrated by the increase in friction for large sliding speeds. As seen in **figure 2B**, a lower friction was measured for b-TPUe, with average friction coefficients (μ) under 0.1, followed by PCL and PLA, with average μ above 0.1.

2.3. Compression test

The mechanical behaviour of b-TPUe was examined and compared with human articular cartilage, PCL, and PLA. The compression curves of PLA, PCL, b-TPUe and cartilage are shown in **figure 2C**. These strongly non-linear curves clearly demonstrate that b-TPUe is more compliant than the other materials investigated (PLA and PCL). Also, unlike PLA and PCL, results for solid (s) and porous (p) b-TPUe scaffolds showed different behaviours in compression. Interestingly, porous b-TPUe scaffolds were significantly softer than their solid counterparts, suggesting that b-TPUe scaffold elasticity can be tailored by changing the porosity. So, b-TPUe scaffolds with greater porosity present a mechanical behaviour closer to the one of native cartilage. In addition, for low strains ε, the mechanical behaviour of b-TPUe was closer to that observed in natural cartilage when compared with PCL or PLA. Moreover, the shear moduli obtained in the second interval of the test showed a clear correlation with the compression data, again demonstrating that b-TPUe exhibited a much lower storage modulus in contrast to the conventional plastics, PCL and PLA **(Figure 2D)**.

2.4. Effects of b-TPUe-conditioned medium on MSCs proliferation

We conducted a proliferation assay to evaluate if the exposure to b-TPUe could have a negative effect in the proliferative potential of MSCs. Results showed no adverse effects in the proliferative potential of MSCs cultured in b-TPUe-conditioned medium for 7 days when compared with MSCs cultured with control medium **(Figure 3A)**.

2.5. Proliferation and viability of MSCs cultured in b-TPUe bioprinted scaffolds

Cell proliferation of MSCs cultured in b-TPUe bioprinted scaffolds was evaluated with an AlamarBlue® assay. PCL filament was used as a control material since it is a reference biomaterial used in cartilage bioprinting (34–37). As can be observed in **figure 3B**, cell proliferation increased from day 1 to day 21 with a significant increase at day 7 of culture in both bioprinting materials, while at day 21 no significant differences were observed in the proliferation rate between cells printed in b-TPUe and those in PCL control scaffolds **(Figure 3B)**.

The viability of MSCs was also evaluated to validate the biocompatibility of b-TPUe printed scaffolds using a live/dead assay. Confocal images **(Figure 3C)** show a majority of green viable MSCs covering both b-TPUe and PCL scaffold fibre surfaces at day 7 and 21 after bioprinting that indicates that b-TPUe bioprinted scaffolds can supports MSCs growth in a same manner as PCL.

2.6. Chondrogenic differentiation of MSCs cultured in b-TPUe bioprinted scaffolds

The MSCs employed in this study were isolated from human adipose tissue. Differentiation potential and phenotypic characterization of isolated MSCs are shown in supplementary Figure 1B. To investigate the capacity of b-TPUe scaffolds to support the induction

of cartilage-like phenotype, chondrogenic key markers were evaluated by RT-PCR after 21 days of culture of bioprinted cell-seeded b-TPUe scaffolds under chondrogenic conditions. Cells extracted from b-TPUe bioprinted scaffolds cultured under chondrogenic media showed a significant increment in type II collagen, aggrecan and Sox9 gene expression when compared with cells grown in monolayer and onto b-TPUe scaffolds without chondrogenic media **(Figure 4A)**.

The ECM produced under induction of chondrogenic differentiation was evaluated assessing glycosaminoglycans (GAGs) and type II collagen concentration in cell culture supernatants of MSCs monolayers and printed MSCs b-TPUe scaffolds cultured with (Diff) or without (CTL) chondrogenic medium for 21 days. The GAGs analysis showed that b-TPUe printed scaffolds in chondrogenic conditions produced a high significant number of GAGs compared to control b-TPUe scaffolds or monolayer conditions **(Figure 4B)**. Similarly, collagen type II production was also markedly greater in b-TPUe printed scaffolds cultured under chondrogenic conditions at 21 days compared to control b-TPUe scaffolds and monolayer conditions **(Figure 4C)**.

Moreover, SEM images showed cell growth and wide cell spread throughout the scaffold over the b-TPUe filament after 21 days of cell growth with and without differentiation conditions. It is relevant to note that cells attached to the filament surface and junctions *via* formation of filopodia and started to form a network of cell and matrix **(Figure 4D-F)**. Also, an enhanced cell growth that covered the pore spaces **(Figure 4G-H)** and over the filament surfaces was observed **(Figure 4I)**.

2.7. *In vivo* assay

Biocompatibility of cell-free b-TPUe scaffolds was assessed *in vivo* by subcutaneous *in situ* implantation in the back of immunocompetent CD-1 mice using PCL as control material **(Figure 5A-D)**. During the study, no cases of mice showing pain behaviour that could be induced by the scaffold implantation or infection were observed. The scaffolds were excised 21 days after implantation, and both scaffolds and mice were photographed to evaluate their appearance and integration within the subcutaneous surrounding tissue. Both b-TPUe and PCL scaffolds were firmly anchored and integrated within the subcutaneous tissue maintaining their shape and integrity. Moreover, no sign of oedema or macroscopic inflammation was detected **(figure 5B and 5D)**.

To assess the integration of the scaffolds within the surrounding tissue, both b-TPUe-MSCs and PCL- MSCs bioprinted scaffolds cultured for 21 days were transplanted into subcutaneous tissue on the flanks of immunodeficient NSG mice, as well as b-TPUe and PCL cell-free scaffolds, and harvested 3 weeks later for subsequent analysis. The implanted bioprinted cell-laden scaffolds showed good integration at the surrounding tissue 21 days post implantation **(Figure 6A)**. Moreover, cell-free scaffolds showed that host cells infiltrated, and grew into the scaffold. Toluidine blue staining demonstrated the presence of GAGs in both b-TPUe and PCL scaffolds. Masson´s Trichrome staining showed that the deposition of collagenous fibres occurred in both materials and in both cell-free and cell-laden conditions **(Figure 6B)**.

3. Discussion

The 3D bioprinting technology allows high precision, fabrication, and customized production, which are important features for biomedical applications. Traditional methods for scaffold manufacturing comprise phase separation (38), electrospinning (39), freeze-drying (40),

and gas forming (41). Comparing this methods to 3D bioprinting, they lack a high precision control of the pore size and shape (42).

In this study, a polyurethane-based 3D printing material, b-TPUe, was successfully used to fabricate scaffolds by 3D bioprinting that were able to maintain cellular viability and growth. We selected the b-TPUe since it belongs to the polyurethane thermoplastics, an adaptable category of materials broadly used for biomedical purposes thanks to their biocompatibility, elasticity and strength (43–47). Other materials which are designed to fill and integrate irregular cartilage wounds, and are also already being tested in clinical trials (48), such us PEG-based adhesive-hydrogels composites, however, they do not show similar mechanical properties to native cartilage, because they previously have to maturate and produce ECM with the same properties of the surrounding healthy tissue. Moreover, to be immobilized on the tissue surface of the lesion they need of a light-initiated reaction to cross-link the liquid polymer solution. In contrast, our b-TPUe polymer can be used to bioprint personalized scaffolds adapted to the shape of the patient lesion. In fact, polyurethane based materials are already being tested in clinical trials (49,50). 3D bioprinting technology allows us to fabricate b-TPUe scaffolds with the desired thickness of fibre and pore size, biomimicking the tissue microstructure, and thus ameliorating the integration of the scaffold within the specific location. The porosity and interconnectivity of the scaffold plays a significant role in nutrient supply, gas diffusion and metabolic waste removal (51,52). Therefore, cells can penetrate the pores following their growth on the scaffold (53).

A selected biomaterial for treating joint replacements is expected to preserve the remaining native cartilage from degradation while maintaining the frictional properties of the joint (54). Analysing the friction profile of the studied materials, b-TPUe showed to exert less friction towards the native cartilage surface than PLA and PCL, showing μ values closer to the cartilage-

to-cartilage interaction (55). Also, the mechanical properties of a scaffold are important for engineering tissues, especially for cartilage, which is subjected to cyclic mechanical forces (56). Although scaffolds based on hydrogels mimic more adequately the mechanical properties found in native tissues (57), their compressive modulus are typically an order of magnitude less than native cartilage tissue (58,59). Otherwise, scaffolds produced with thermoplastics possess higher Young's modulus than those based on hydrogels (60,61). The obtained results suggests that b-TPUe scaffold elasticity can be tailored, by changing the porosity, to achieve a closer values to the natural cartilage Young's modulus than hydrogel scaffolds and synthetic polymers such as PCL or PLA (57), thus exhibiting promising customizable mechanical properties. The viscoelastic modulus in scaffold-based TE is important to approximate and supply the unique properties of the normal articular cartilage that is trying to be replaced (62). The ideal scaffold for cartilage regeneration is a material with viscoelastic and hydrodynamic properties that mimic the mechanical microenvironment of cartilage matrix, which could provide proper mechanical and biochemical signals for chondrocyte adhesion proliferation, differentiation, and ECM formation. (63). Moreover, this similarity to the natural viscoelastic properties and compliance with dynamic environments is important for the integration without damaging the surrounding tissue. In fact, recent researches noticed the importance of material viscoelasticity in cartilage tissue engineering (64,65), since viscoelastic matrix with stress relaxation could mimic the mechanical microenvironment of soft tissues, and thus favour chondrogenic differentiation and a better integration with the cartilage (66).

Biocompatibility must be a priority when selecting biomaterials for TE (67). Polyurethanes are considered to have good biocompatibility properties and are widely used for long-term medical implants, such as cardiac pacemakers and vascular grafts (68). Since b-TPUe is a recently

developed polyurethane-based 3D printing filament, no previous data concerning the possible cytotoxicity of this material on cell growth has been previously published. Results of the cytotoxicity, proliferation and viability assays, showed no cytotoxic effects of b-TPUe and that it can provide an environment that supports MSCs proliferation in a same manner as PCL (69). In fact, large spaces between the fibres allowed the adhered cells to start accommodating between the stacking fibres.

Regarding cartilage ECM production, expression of type II collagen and aggrecan, which are the main proteins of the hyaline cartilage ECM (70), showed to be upregulated in cells cultured in b-TPUe scaffold under chondrogenic media compared with control conditions. Similarly, Sox9, which is a known transcription factor of chondrogenesis that acts in the early stages of chondrogenic differentiation inducing type II collagen production (71) also showed to be upregulated. In addition, non-increased expression of collagen type I in b-TPUe scaffolds under chondrogenic media compared with their counterparts cultured in non-differentiated media or cells cultured in monolayer without chondrogenic media was observed. Type I collagen has been described in fibroblastic differentiation and could indicate the formation of fibrous cartilage (72). The upregulation of chondrogenic genes, together with the low expression of collagen type I of MSCs bioprinted in b-TPUe scaffolds, indicate the ability of this material to support the differentiation of MSCs into chondrocyte-like cells. In accordance with these results, an increased GAGs and collagen type II deposition in the ECM of b-TPUe MSCs bioprinted scaffolds cultured under chondrogenic conditions indicated the development of a cartilaginous-like matrix (73). This chondrogenic support of b-TPUe MSCs bioprinted scaffolds are in agreement with those previously obtained for PCL (74). Further studies are necessary to compare the MSCs

chondrogenesis of b-TPUe with other biomaterials such as PCL, PLA or PEG-based hydrogels, among others.

In the present study, we tried to evaluate qualitatively the macroscopic response to b-TPUe scaffolds in an *in vivo* environment. The lack of pain behaviour, infection, oedema or macroscopic tissue inflammation during the *in vivo* assay with immunocompetent CD-1 mice, as well as the maintenance of shape and integrity of the scaffold, and its integration within the implantation surrounding tissue indicate the *in vivo* biocompatibility of b-TPUe as previously described for other 3D polyurethanes (75). Similarly, when implanted in immunodeficient NSG mice, the deposition of collagenous fibers in both cell-free and cell-laden scaffolds suggest that b-TPUe can allow *in vivo* GAGs and collagenous fibre production as well as PCL. Thus, it can be stated that b-TPUe polymer scaffolds showed good *in vivo* ECM deposition confirming the integration of b-TPUe within the host's tissue (76).

3. Conclusion

In this study, a novel elastic polyurethane-based 3D printing material, b-TPUe, was successfully used to fabricate 3D printed scaffolds with improved rheological and tribological properties compared to PCL and PLA. This new printing material, besides showing the ability to support the growth and chondrogenic differentiation of MSCs, also presents a mechanical behaviour closer to natural cartilage when compared with PCL and PLA. Interestingly, the elastic characteristics of b-TPUe changes when modifying the porosity, improving the customization of the mechanical properties of the constructs, therefore offering the possibility to better adapt this parameter to the desired target tissue. Moreover, b-TPUe showed a tribological performance closer to cartilage in comparison to PLA and PCL, suggesting that it is an appropriate material to be used in cartilage replacement to restore joint function. Furthermore, b-TPUe demonstrated a high

biocompatibility when growing MSCs onto b-TPUe scaffolds. In fact, b-TPUe bioprinted scaffolds were found to support MSCs proliferation and the upregulation of hyaline-like cartilage tissue markers in their gene expression, with no *in vivo* toxic effects. These results highlight the potential of b-TPUe as a 3D printing material with application in cartilage TE. In addition, the development of materials such as b-TPUe that allow the scaffold customization is essential for other soft tissues such as such as tendon, muscle, or ligaments. Moreover, due to the excellent biomechanical properties and biocompatibility, we have set the basis for further exploration of this novel material for biomedical and tissue regenerative applications.

4. Experimental Section

Patients: Human infrapatellar fat pad, cartilage tissue and synovial fluid were obtained from patients with knee OA during joint replacement surgery. Ethical approval for the study was obtained from the Ethics Committee of the Clinical University Hospital of Málaga, Spain (ethic permission number: 02/022010 Hospital Virgen de la Victoria, Málaga). Informed patient consent was obtained for all samples used in this study. None of the patients had a history of inflammatory arthritis or crystal-induced arthritis. Hoffa's fat pad was harvested from the inside of the capsule excluding vascular areas and synovial regions. Human articular cartilage was obtained from the femoral side, selecting the non-overload compartment. Only cartilage that looked normal macroscopically was used for this study. Samples collected at joint arthroplasty were transported to the laboratory in Dulbecco's modified Eagle's medium (DMEM; Sigma, St. Louis, MO, USA) with 1% penicillin/streptomycin (P/S). Synovial fluid (SF) was pooled from knee joints and mixed on an orbital shaker. Only samples that were free of blood contamination were used, as assessed visually. SF was stored at -20°C between testing sessions (77).

Isolation and culture of human MSCs from infrapatellar fat pad: Infrapatellar fat pad tissue was minced and digested with an enzymatic solution of 1 mg/mL collagenase type IA (Sigma) and incubated in shaking at 37ºC for 1 h. Once digested, collagenase was removed with a single wash of sterilized phosphate-buffered saline (PBS), followed by two washes of DMEM supplemented with 10% foetal bovine serum (FBS) (Sigma). The cell pellet was resuspended in DMEM supplemented with 10% FBS and 1% Penicilin/Sreptomycin, placed into tissue culture flasks, and cultured at 37 ºC in a 5% CO_2 atmosphere. After 48 h the medium was removed to discard non-adherent and dead cells (78). When 80% of confluence was reached, cells were released with Tryple Express (Gibco) and sub-cultured. Phenotype and differentiation potential of isolated MSCs were characterised, as previously described (78,79). To examine their immunophenotype, MSCs were harvested, rinsed twice in PBS, and blocked with bovine serum albumin (BSA) 1% in PBS for 10 min at room temperature (RT). Fluorescent monoclonal antibodies CD73, CD90 and CD105 antibodies were used as positive markers, while CD34, CD45 and HLA-DR antibodies were used as negative markers (80). Antibodies were incubated at dark for 15 min at 4 ºC. Before their analysis, MSCs were washed twice with PBS to remove non-bound antibodies. Flow cytometry analysis was performed with a BD FACSCantoTM II cytometer (BD Biosciences, CA, USA) and the resulting data were analyzed using the FACSDivaTM software (BD Biosciences). For the differentiation assays, MSCs were plated at 1×10^5 cells/ cm^2 in DMEM-FBS into 6-well culture plates. After 48 h, the culture medium was replaced with specific differentiation-inductive medium. For adipogenic, osteogenic and chondrogenic differentiation, MSCs were cultured for 2 weeks in MSC Adipogenic Differentiation BulletKit™ (Lonza, Basilea, Switzerland), MSC Osteogenic Differentiation BulletKit™ (Lonza) and StemMACS ChondroDiff Medium (Miltenyi Biotec, Bergisch Gladbach, Germany), respectively. Differentiated cell cultures were stained with

oil red O (Amresco, Solon, OH, USA) for adipogenic differentiation, alizarin red (Lonza) for osteogenic differentiation or toluidine blue (Sigma-Aldrich) for chondrogenic differentiation.

Bioprinting process: A Regemat 3D V1 bioprinter (REGEMAT 3D S.L., Spain) was used for 3D printing with a direct extruder to fabricate the scaffolds (81). Commercial PCL (3D4Makers, 1.75 mm filament, printing temperature: 70 - 90 ºC; semi-crystalline aliphatic polyester) was melted at 75 ºC and printed at rate of 1.1 mm/s. Commercial PLA (Smart materials 3D, Spain, 1.75 mm filament, printing temperature: 190 - 210 ºC; polymerized polylactic acid) was melted at 200 ºC and printed at rate of 1.2 mm/s. Commercial b-TPUe (Recreus industries s.l., 1.75 mm filament, printing temperature: 200 - 230 ºC; based on methylene diphenyl diisocyanate (MDI) and 1,4-Butanediol) was melted at 200 ºC and printed at rate of 1.4 mm/s. Printing parameters were optimized for each material in order to obtain the best printability and scaffold quality layout. PCL, PLA and b-TPUe scaffolds were designed to be extruded with triangular patterns for the infill with a pore size of 0.6 mm, solid walls consisting of a perimeter of 0.4 mm width, and 3 solid layers for the bottom, with a 0.2 mm layer height (Figure 1A). The scaffolds were printed as 3D cylindrical frameworks in a triangular inner lattice from alternately stacking filament fibres (Figure 1B). For 3D bioprinting with cells, the Regemat 3D V1 bioprinter was placed in a laminar flow hood. In the same process, the thermal extruder unit of the bioprinter was used to print the scaffolds, and then the syringe unit of the bioprinter was used to seed the cell suspension into the porous structure with a 200 µm diameter needle (1×10^5 cells/scaffold). PCL was used as a control material instead of PLA as it is more used for biomedical purposes than its counterpart. For all *in vitro* assays the scaffold dimensions were designed to fit in a 24-well plate (10 mm in diameter and 3 mm in height; 15 layers), with smaller dimensions for the *in vivo* assays (5 mm in diameter and 3 mm in height; 15 layers). Once bioprinted, the scaffolds were introduced in a 24-well plate

and incubated for at least 1 h to allow the cells to adhere to the fibres. Finally, the scaffolds were submerged in culture medium containing DMEM supplemented with 10% FBS and 1% P/S and then, stored at 37 ºC in a 5% CO_2 atmosphere. Scaffolds used to support MSCs chondrogenic differentiation were cultured in DMEM supplemented with 10% FBS, 1% P/S, 50 μg/μL l-ascorbic acid 2-phosphate (Sigma), 40 μg/mL proline (Sigma), 1% insulin-transferrin-selenium (ITS) (Gibco), 40 μg/μL L-proline (Sigma), and 10 ng/mL transforming growth factor β3 (TGF-β3) (82).

Tribological tests: A ball-on-three plates tribometer was adapted to a rheometer (Anton Paar, Austria) to interrogate the lubricating behaviour of the different materials. The contact consisted in a plastic ball (made of PLA, PCL or b-TPUe) that slides along three cartilage surfaces (cartilage disks with a diameter of 5 mm) lubricated by synovial fluid. The MCR501 rheometer head (Anton Paar) was used to calculate the friction coefficient. A schematic diagram of the test set-up is shown in Figure 2A. In this set-up, a ball is pressed at a given normal force F_N against three plates that are mounted on a movable stage. The experimental protocol was as follows. First, the test rig was assembled, and 400 μL of SF was added. This amount was enough to fully immerse the three-point contacts to a depth of 1 mm. Next, temperature was stabilized at 25 ºC and the plastic ball was loaded against the cartilage plates. Then, the ball was made to slide over the plates at a controlled (decreasing) speed V, from 2500 to 0.1 rpm under a normal force of F_N = 1 N (5 s per data point), while the resulting torque T sensed by the ball was monitored. The friction coefficient μ was computed with $\mu = T/(F_N R)$ being R the radius of the ball.

Rheological assays: Specimens for rheological assays were printed with 20 mm in diameter and 5 mm in height, solids and porous to analyse the effect of the infill over the mechanical characteristics of the scaffold (n = 3). Porous samples were printed with the same pattern of the ones used for cell culture tests. A MCR302 (Anton Paar) head was used to carry out rheological

measurements at 25 ºC. A three-step test was designed to obtain information on the compression and shearing characteristics of specimen. First, the scaffold was placed onto the base of the rheometer. Then, the rheometer head was approached at a constant speed (10 µm/s) up to a normal force of 40 N. Next, the specimen was oscillatory sheared according to a strain amplitude of 0.00001% at a frequency of 1 Hz and normal force of 40 N to determine the shear viscoelastic moduli and, finally, the upper plate was separated at a constant speed (10 µm/s).

Cell viability assay: Cell viability in the 3D printed scaffolds was determined on days 7 and 21 after bioprinting using Live/Dead™ Viability/Cytotoxicity Kit (Invitrogen). The printed constructs were incubated in PBS containing calcein AM (2µM) and ethidium homodimer (4 µM) at 37 ºC for 30 min to stain live and dead cells (83). Scaffolds were imaged by confocal microscopy (Nikon Eclipse Ti-E A1, Amsterdam, Netherlands) and analysed using NIS-Elements software (Amsterdam, Netherlands).

Scanning electron microscopy (SEM): The morphology and structure of b-TPUe scaffolds were analysed using a variable-pressure and environmental scanning electron microscope (ESEM) FEI, mod. Quanta 400 (Oregon, USA). The analysis was performed in high vacuum mode to characterize the surface structure of scaffolds and cell growth. Samples were fixed with 2% glutaraldehyde and then, were rinsed in 0.1 M cacodylate buffer and incubated overnight at 4 °C. For critical point, the samples were then maintained with Osmium tetroxide 1% RT during 1h and dehydrated in a series of ethanol solutions (50%, 70%, 90%, 100%, 100%, 100%), by soaking the samples in each solution for 15 min. Subsequently, samples were critical point dried (Anderson, 1951) in a desiccator (Leica EMCPD300), and covered by evaporating them in a carbon evaporator (Emitech K975X).

In vitro cytotoxicity test: MSCs culture medium aliquots were conditioned with b-TPUe samples as previously described (84). Briefly, b-TPUe sterilized scaffolds for a total mass of 3 g were placed in T-75 tissue culture flasks and soaked in 100 mL of complete cell culture medium for 10 days at 37 °C in a cell culture incubator on a rocking platform. Control medium was incubated in parallel, but without the b-TPUe scaffolds. MSCs were plated in a 6-well plate at 1 x 10^5 cells/well. After 24 h the medium was replaced with a mix of a 1:1 fresh medium: b-TPUe-conditioned medium or with fresh control medium. Cell growth was analysed at different time points: 1, 3, 5 and 7 days using AlamarBlue® assay (Bio-Rad Laboratories, Inc., manufactured by Trek Diagnostic System. U.S.). Cells were incubated with AlamarBlue® solution at 37 ºC for 3 h. Fluorescence of reduced AlamarBlue® was determined at 530/590 nm excitation/emission wavelengths (Synergy HT, BIO-TEK).

Cell proliferation assay: Cell proliferation was analyzed using AlamarBlue® assay after 1, 3, 5, 7, 14 and 21 days. The scaffolds were incubated with AlamarBlue® solution at 37 ºC for 3 h. Fluorescence of reduced AlamarBlue® was determined at 530/590 nm excitation/emission wavelengths.

RNA isolation and real time-PCR analysis: Total cellular RNA was isolated using TriReagent (Sigma) and reverse transcribed using the Reverse Transcription System kit (Promega). Real-time PCR was performed using the SYBR-Green PCR Master mix (Promega) according to the manufacturer's recommendations. PCR reactions were performed as follows: an initial denaturation at 95 °C for 2 min, 40 cycles of 95 °C for 5 s followed by 60 °C for 30 s, and final cycle of dissociation of 60 – 95 °C. The gene expression levels were normalized to corresponding GAPDH values and are shown as relative fold expression to the control sample. All samples were analysed in triplicate for each gene. Primer sequences used are shown in Table 1.

Glycosaminoglycan quantification: The dimethylmethylene blue (DMMB) assay was used to study the glycosaminoglycans (GAGs) content as previously described (85). Briefly, 50 µL of papain-digested sample harvested at day 21 were added in triplicate to a 96-well plate and combined with 200 µL of DMMB dye, and the absorbance at 540 nm was immediately read. To determine the GAGs content of the samples chondroitin sulphate from shark cartilage (Sigma) was used as standard.

Type II Collagen quantification: Type II collagen content produced in the scaffolds was quantified by ELISA (Type II Collagen Detection kit #6018; Chondrex, Redmond, WA) according to manufacturer's instruction. Briefly, samples were digested using pepsin in 0.5 M acetic acid: collagen ratio of 1:10 (w/w) for 2 days. Once digested, samples were incubated at 4 ºC overnight in elastase: collagen ratio of 1:10 (w/w). Then, standard and samples were placed in a pre-coated 96-well plate with capture antibodies and incubated for 30 min. The detection antibody was added and incubated for 1.5 h and then washed. The plate was incubated with streptavidin peroxidase for 1 h, washed, and incubated with ortho-phenyldiamine (OPD) solution for 30 min. A solution of 2N sulphuric acid was added to stop the reaction, and the content of type II collagen was quantified by absorbance at 490 nm.

In vivo assays: *In vivo* assays were carried out in accordance with the approved guidelines of University of Granada following institutional and international standards for animal welfare and experimental procedure. The Research Ethics Committee of the University of Granada approved all experimental protocols. Experiments were performed in immunocompetent CD-1 mice and immunodeficient NOD SCID (NOD.CB17-Prkdcscid/NcrCrl) (NSG) mice purchased from Charles River (Barcelona, Spain). To evaluate the biocompatibility, PCL and b-TPUe cell-free scaffolds were transplanted into two independent small subcutaneous pockets made on the back of

CD-1 mice anesthetized by isoflurane inhalation (n = 5 per group). In addition, MSCs cell-laden scaffolds cultured for 21 days were implanted into two independent small subcutaneous pockets created on the back of NSG mice anesthetized by isoflurane inhalation to evaluate engraftment. Cell-laden or cell-free scaffolds were implanted in each pocket with a single biomaterial per mouse (b-TPUe or PCL) (n = 5 per group). Animals were maintained in a microventilated cage system with a 12-h light/dark cycle with food and water *ad libitum*. Mice were manipulated within a laminar airflow hood to maintain pathogen-free conditions. Three weeks later, mice were sacrificed *via* an overdose injection of an aesthetic, and the scaffolds were photographed to evaluate the implantation within the surrounding mouse tissue and recovered for histological analyses. For the histological analysis, samples were dehydrated, embedded in Technovit 7200 and polymerized. The blocks were sectioned with a diamond-coated band saw (Exakt 310 CP) and then, grounded, and polished with a high precision grinder (Exakt 400). The total histological processing, including Toluidine Blue and Masson staining, were performed by Histology Unit of BIONAND (Málaga, Spain) following the Donath and Bruener cutting/grinding technique (86).

Statistical analysis: Statistical calculations were performed using SPSS 13.0 software for Windows (SPSS, Chicago, IL, USA). All graphed data represent the mean +/- SD from at least three experiments. Differences between treatments were tested using the two-tailed Student´s T test. Assumptions of Student´s T test (homoscedasticity and normality) were tested and assured by using transformed data sets [log(dependent variable value + 1)] when necessary. P-values < 0.05 (*) and P-values < 0.01 (**) were considered statistically significant in all cases.

Funding Sources

This research was supported by MINECO MAT 2016-78778-R and PCIN-2015-051 projects (Spain), European Regional Development Fund (ERDF), by the Consejería de Economía, Conocimiento, Empresas y Universidad de la Junta de Andalucía and European Regional Development Fund (ERDF), ref. SOMM17/6109/UGR, and by the Fundación Mutua Madrileña (project FMM-AP17196-2019).

Acknowledgments

The authors gratefully thank Ana Santos and Mohamed Tassi from the C.I.C. (University of Granada) for excellent technical assistance with microscopy studies and acknowledge Isabel Sánchez-Almazo from the C.I.C. (University of Granada) for excellent technical assistance with SEM studies.

Conflict of Interest Declaration

The authors declare no conflicts of interest.

Abbreviations

b-TPUe, 1,4-Butanediol thermoplastic polyurethane; TE, tissue engineering; PCL, poly-ε-caprolactone; PLA, poly-L-lactic acid; MSCs, mesenchymal stem cells; OA, osteoarthritic; CAD, computer-aided design; CAM, computer-aided manufacturing; SLA, stereolithography; ECM, extracellular matrix; PLGA, polylactic-co-glycolic acid; SEM, Scanning electron microscope; GAGs, glycosaminoglycans; PBS, phosphate-buffered saline; FBS, fetal bovine serum; ITS, insulin-transferrin-selenium; TGF-β3, transforming growth factor β3; ESEM, environmental scanning electron microscope; DMMB, dimethylmethylene blue; OPD, ortho-phenyldiamine.

REFERENCES

1. Derakhshanfar S, Mbeleck R, Xu K, et al. 3D bioprinting for biomedical devices and tissue engineering: A review of recent trends and advances. *Bioact Mater*. 2018 Jun 1;3(2):144–56.
2. Hutmacher DW, Sittinger M, Risbud M V. Scaffold-based tissue engineering: rationale for computer-aided design and solid free-form fabrication systems. *Trends Biotechnol*. 2004 Jul 1;22(7):354–62.
3. Ozler SB, Bakirci E, Kucukgul C, et al. Three-dimensional direct cell bioprinting for tissue engineering. *J Biomed Mater Res Part B Appl Biomater*. 2017 Nov;105(8):2530–44.
4. Zhang YS, Yue K, Aleman J, et al. 3D Bioprinting for Tissue and Organ Fabrication. *Ann Biomed Eng*. 2017;45(1):148–63.
5. Bishop ES, Mostafa S, Pakvasa M, et al. 3-D bioprinting technologies in tissue engineering and regenerative medicine: Current and future trends. *Genes Dis*. 2017 Dec;4(4):185–95.
6. Hölzl K, Lin S, Tytgat L, et al. Bioink properties before, during and after 3D bioprinting. *Biofabrication*. 2016 Sep 23;8(3):032002.
7. Seliktar D. Designing Cell-Compatible Hydrogels for Biomedical Applications. *Science (80-)*. 2012 Jun 1;336(6085):1124–8.
8. Senatov FS, Niaza KV, Zadorozhnyy MY, et al. Mechanical properties and shape memory effect of 3D-printed PLA-based porous scaffolds. *J Mech Behav Biomed Mater*. 2016 Apr;57:139–48.
9. Diomede F, Gugliandolo A, Cardelli P, et al. Three-dimensional printed PLA scaffold and human gingival stem cell-derived extracellular vesicles: a new tool for bone defect repair. *Stem Cell Res Ther*. 2018 Dec 13;9(1):104.

10. Grémare A, Guduric V, Bareille R, et al. Characterization of printed PLA scaffolds for bone tissue engineering. *J Biomed Mater Res Part A*. 2018 Apr;106(4):887–94.
11. Gregor A, Filová E, Novák M, et al. Designing of PLA scaffolds for bone tissue replacement fabricated by ordinary commercial 3D printer. *J Biol Eng*. 2017 Dec 16;11(1):31.
12. Shkarina S, Shkarin R, Weinhardt V, et al. 3D biodegradable scaffolds of polycaprolactone with silicate-containing hydroxyapatite microparticles for bone tissue engineering: high-resolution tomography and in vitro study. *Sci Rep*. 2018 Dec 11;8(1):8907.
13. Su Y, Denbeigh JM, Camilleri ET, et al. Extracellular matrix protein production in human adipose-derived mesenchymal stem cells on three-dimensional polycaprolactone (PCL) scaffolds responds to GDF5 or FGF2. *Gene Reports*. 2018 Mar;10:149–56.
14. Kim J-Y, Ahn G, Kim C, et al. Synergistic Effects of Beta Tri-Calcium Phosphate and Porcine-Derived Decellularized Bone Extracellular Matrix in 3D-Printed Polycaprolactone Scaffold on Bone Regeneration. *Macromol Biosci*. 2018 Jun;18(6):1800025.
15. Dao TT-T, Vu NB, Pham LH, et al. In Vitro Production of Cartilage Tissue from Rabbit Bone Marrow-Derived Mesenchymal Stem Cells and Polycaprolactone Scaffold. In: Advances in experimental medicine and biology. 2017.
16. Park K-S, Kim B-J, Lih E, et al. Versatile effects of magnesium hydroxide nanoparticles in PLGA scaffold–mediated chondrogenesis. *Acta Biomater*. 2018 Jun;73:204–16.
17. Lin S, Cui L, Chen G, et al. PLGA/β-TCP composite scaffold incorporating salvianolic acid B promotes bone fusion by angiogenesis and osteogenesis in a rat spinal fusion model. *Biomaterials*. 2018 Apr 4;
18. Brown JH, Das P, DiVito MD, et al. Nanofibrous PLGA electrospun scaffolds modified with type I collagen influence hepatocyte function and support viability in vitro. *Acta*

Biomater. 2018 Jun;73:217–27.

19. Dai Y, Shen T, Ma L, et al. Regeneration of osteochondral defects in vivo by a cell-free cylindrical poly(lactide-co-glycolide) scaffold with a radially oriented microstructure. *J Tissue Eng Regen Med*. 2018 Mar;12(3):e1647–61.
20. Serra T, Mateos-Timoneda MA, Planell JA, et al. 3D printed PLA-based scaffolds: a versatile tool in regenerative medicine. *Organogenesis*. 2013;9(4):239–44.
21. Maggi A, Li H, Greer JR. Three-dimensional nano-architected scaffolds with tunable stiffness for efficient bone tissue growth. *Acta Biomater*. 2017 Nov 1;63:294–305.
22. Serrano MC, Chung EJ, Ameer GA. Advances and Applications of Biodegradable Elastomers in Regenerative Medicine. *Adv Funct Mater*. 2010 Jan 22;20(2):192–208.
23. Zheng MH, Willers C, Kirilak L, et al. Matrix-Induced Autologous Chondrocyte Implantation (MACI®): Biological and histological assessment. *Tissue Eng*. 2007 Apr;13(4):737–46.
24. Legendre F, Ollitrault D, Hervieu M, et al. Enhanced hyaline cartilage matrix synthesis in collagen sponge scaffolds by using siRNA to stabilize chondrocytes phenotype cultured with bone morphogenetic protein-2 under hypoxia. *Tissue Eng - Part C Methods*. 2013 Jul 1;19(7):550–67.
25. Willers C, Chen J, Wood D, et al. Autologous chondrocyte implantation with collagen bioscaffold for the treatment of osteochondral defects in rabbits. In: Tissue Engineering. Tissue Eng; 2005. p. 1065–76.
26. Bentley G, Biant LC, Vijayan S, et al. Minimum ten-year results of a prospective randomised study of autologous chondrocyte implantation versus mosaicplasty for symptomatic articular cartilage lesions of the knee. *J Bone Jt Surg - Ser B*. 2012 Apr;94

B(4):504–9.

27. Vinatier C, Guicheux J. Cartilage tissue engineering: From biomaterials and stem cells to osteoarthritis treatments. Vol. 59, Annals of Physical and Rehabilitation Medicine. Elsevier Masson SAS; 2016. p. 139–44.

28. Chaudhari AA, Vig K, Baganizi DR, et al. Future prospects for scaffolding methods and biomaterials in skin tissue engineering: A review [Internet]. Vol. 17, International Journal of Molecular Sciences. MDPI AG; 2016.

29. Armiento AR, Stoddart MJ, Alini M, et al. Biomaterials for articular cartilage tissue engineering: Learning from biology. Vol. 65, Acta Biomaterialia. Acta Materialia Inc; 2018. p. 1–20.

30. Jaganathan SK, Mani MP, Supriyanto E. Blood compatibility assessments of electrospun polyurethane nanocomposites blended with megni oil for tissue engineering applications. *An Acad Bras Cienc*. 2019 Jun 19;91(2):e20190018.

31. Ergene E, Yagci BS, Gokyer S, et al. A novel polyurethane-based biodegradable elastomer as a promising material for skeletal muscle tissue engineering. *Biomed Mater*. 2019 Feb 25;14(2):025014.

32. Ma Y, Hu N, Liu J, et al. Three-Dimensional Printing of Biodegradable Piperazine-Based Polyurethane-Urea Scaffolds with Enhanced Osteogenesis for Bone Regeneration. *ACS Appl Mater Interfaces*. 2019 Mar 6;11(9):9415–24.

33. Blaya F, Pedro PS, Pedro ABS, et al. Design of a Functional Splint for Rehabilitation of Achilles Tendon Injury Using Advanced Manufacturing (AM) Techniques. Implementation Study. *J Med Syst*. 2019 May 1;43(5).

34. Petrie Aronin CE, Cooper JA, Sefcik LS, et al. Osteogenic differentiation of dura mater

stem cells cultured in vitro on three-dimensional porous scaffolds of poly(ε-caprolactone) fabricated via co-extrusion and gas foaming. *Acta Biomater*. 2008 Sep;4(5):1187–97.

35. Kim H-J, Lee J-H, Im G-I. Chondrogenesis using mesenchymal stem cells and PCL scaffolds. *J Biomed Mater Res Part A*. 2009;9999A:NA-NA.

36. Izquierdo R, Garcia-Giralt N, Rodriguez MT, et al. Biodegradable PCL scaffolds with an interconnected spherical pore network for tissue engineering. *J Biomed Mater Res Part A*. 2008 Apr;85A(1):25–35.

37. Li W-JW-J, Tuli R, Okafor C, et al. A three-dimensional nanofibrous scaffold for cartilage tissue engineering using human mesenchymal stem cells. *Biomaterials*. 2005 Feb;26(6):599–609.

38. Wei G, Ma PX. Partially nanofibrous architecture of 3D tissue engineering scaffolds. *Biomaterials*. 2009 Nov;30(32):6426–34.

39. Ghosh S, Laha M, Mondal S, et al. In vitro model of mesenchymal condensation during chondrogenic development. *Biomaterials*. 2009 Nov;30(33):6530–40.

40. Zhang Y, Yang F, Liu K, et al. The impact of PLGA scaffold orientation on invitro cartilage regeneration. *Biomaterials*. 2012 Apr;33(10):2926–35.

41. Tai H, Mather ML, Howard D, et al. Control of pore size and structure of tissue engineering scaffolds produced by supercritical fluid processing. *Eur Cells Mater*. 2007;14:64–76.

42. Izadifar Z, Chen X, Kulyk W. Strategic Design and Fabrication of Engineered Scaffolds for Articular Cartilage Repair. *J Funct Biomater*. 2012 Nov 14;3(4):799–838.

43. Bacakova L, Filova E, Parizek M, et al. Modulation of cell adhesion, proliferation and differentiation on materials designed for body implants. *Biotechnol Adv*. 2011 Nov;29(6):739–67.

44. Michael S, Sorg H, Peck CT, et al. Tissue Engineered Skin Substitutes Created by Laser-Assisted Bioprinting Form Skin-Like Structures in the Dorsal Skin Fold Chamber in Mice. *PLoS One*. 2013;8(3).

45. Monllau JC, Poggioli F, Erquicia J, et al. Magnetic Resonance Imaging and Functional Outcomes After a Polyurethane Meniscal Scaffold Implantation: Minimum 5-Year Follow-up. *Arthrosc J Arthrosc Relat Surg*. 2018 May;34(5):1621–7.

46. Shafaat S, Mangir N, Regureos SR, et al. Demonstration of improved tissue integration and angiogenesis with an elastic, estradiol releasing polyurethane material designed for use in pelvic floor repair. *Neurourol Urodyn*. 2018 Feb;37(2):716–25.

47. Mangera A, Bullock AJ, Roman S, et al. Comparison of candidate scaffolds for tissue engineering for stress urinary incontinence and pelvic organ prolapse repair. *BJU Int*. 2013 Sep;112(5):674–85.

48. Sharma B, Fermanian S, Gibson M, et al. Human cartilage repair with a photoreactive adhesive-hydrogel composite. *Sci Transl Med*. 2013 Jan 9;5(167):167ra6-167ra6.

49. Olivos-Meza A, Pérez Jiménez FJ, Granados-Montiel J, et al. First Clinical Application of Polyurethane Meniscal Scaffolds with Mesenchymal Stem Cells and Assessment of Cartilage Quality with T2 Mapping at 12 Months. *Cartilage*. 2019 Aug 7;194760351985241.

50. Bulgheroni P, Bulgheroni E, Regazzola G, et al. Polyurethane scaffold for the treatment of partial meniscal tears. Clinical results with a minimum two-year follow-up. *Joints*. 2013;1(4):161–6.

51. Kumar A, Biswas K, Basu B. Hydroxyapatite-titanium bulk composites for bone tissue engineering applications. *J Biomed Mater Res Part A*. 2015 Feb;103(2):791–806.

52. Habib FN, Nikzad M, Masood SH, et al. Design and Development of Scaffolds for Tissue Engineering Using Three-Dimensional Printing for Bio-Based Applications. *3D Print Addit Manuf*. 2016 Jun 20;3(2):119–27.

53. Theodoridis K, Aggelidou E, Vavilis T, et al. Hyaline cartilage next generation implants from adipose-tissue-derived mesenchymal stem cells: Comparative study on 3D-printed polycaprolactone scaffold patterns. *J Tissue Eng Regen Med*. 2019 Feb 1;13(2):342–55.

54. Stojanović B, Bauer C, Stotter C, et al. Tribocorrosion of a CoCrMo alloy sliding against articular cartilage and the impact of metal ion release on chondrocytes. *Acta Biomater*. 2019 Jun 18;

55. Kanca Y, Milner P, Dini D, et al. Tribological properties of PVA/PVP blend hydrogels against articular cartilage. *J Mech Behav Biomed Mater*. 2018 Feb 1;78:36–45.

56. Patel A, Gaharwar AK, Iviglia G, et al. Highly elastomeric poly(glycerol sebacate)-co-poly(ethylene glycol) amphiphilic block copolymers. *Biomaterials*. 2013 May;34(16):3970–83.

57. Liu J, Zheng H, Poh P, et al. Hydrogels for Engineering of Perfusable Vascular Networks. *Int J Mol Sci*. 2015 Jul 14;16(7):15997–6016.

58. Tatman PD, Gerull W, Sweeney-Easter S, et al. Multiscale Biofabrication of Articular Cartilage: Bioinspired and Biomimetic Approaches [Internet]. Vol. 21, Tissue Engineering - Part B: Reviews. Mary Ann Liebert Inc.; 2015. p. 543–59.

59. Little CJ, Bawolin NK, Chen X. Mechanical properties of natural cartilage and tissue-engineered constructs. *Tissue Eng - Part B Rev*. 2011 Aug 1;17(4):213–27.

60. Fedorovich NE, De Wijn JR, Verbout AJ, et al. Three-Dimensional Fiber Deposition of Cell-Laden, Viable, Patterned Constructs for Bone Tissue Printing. *Tissue Eng Part A*. 2008

Jan;14(1):127–33.

61. Cohen DL, Malone E, Lipson H, et al. Direct freeform fabrication of seeded hydrogels in arbitrary geometries. *Tissue Eng*. 2006;12.

62. Izadifar Z, Chen X, Kulyk W. Strategic Design and Fabrication of Engineered Scaffolds for Articular Cartilage Repair. *J Funct Biomater*. 2012 Nov 14;3(4):799–838.

63. Li C, Wang L, Yang Z, et al. A viscoelastic chitosan-modified three-dimensional porous poly(L-lactide-co-ε-Caprolactone) scaffold for cartilage tissue engineering. *J Biomater Sci Polym Ed*. 2012;23(1–4):405–24.

64. Lee HP, Gu L, Mooney DJ, et al. Mechanical confinement regulates cartilage matrix formation by chondrocytes. *Nat Mater*. 2017 Dec 1;16(12):1243–51.

65. Chaudhuri O, Gu L, Klumpers D, et al. Hydrogels with tunable stress relaxation regulate stem cell fate and activity. *Nat Mater*. 2016 Mar 1;15(3):326–34.

66. Lin D, Cai B, Wang L, et al. A viscoelastic PEGylated poly(glycerol sebacate)-based bilayer scaffold for cartilage regeneration in full-thickness osteochondral defect. *Biomaterials*. 2020 Sep 1;253:120095.

67. Kiradzhiyska DD, Mantcheva RD. Overview of Biocompatible Materials and Their Use in Medicine. *Folia Med (Plovdiv)*. 2019 Mar 1;61(1):34–40.

68. Zdrahala RJ, Zdrahala IJ. Biomedical Applications of Polyurethanes: A Review of Past Promises, Present Realities, and a Vibrant Future. *J Biomater Appl*. 1999 Jul;14(1):67–90.

69. Rashad A, Mohamed-Ahmed S, Ojansivu M, et al. Coating 3D Printed Polycaprolactone Scaffolds with Nanocellulose Promotes Growth and Differentiation of Mesenchymal Stem Cells. *Biomacromolecules*. 2018 Nov 12;19(11):4307–19.

70. Fraser A, Fearon U, Billinghurst RC, et al. Turnover of type II collagen and aggrecan in

cartilage matrix at the onset of inflammatory arthritis in humans: Relationship to mediators of systemic and local inflammation. *Arthritis Rheum*. 2003 Nov 1;48(11):3085–95.

71. Lefebvre V, Huang W, Harley VR, et al. SOX9 is a potent activator of the chondrocyte-specific enhancer of the pro alpha1(II) collagen gene. *Mol Cell Biol*. 1997 Apr;17(4):2336–46.

72. Goldwasser M, Astley T, van der Rest M, et al. Analysis of the type of collagen present in osteoarthritic human cartilage. *Clin Orthop Relat Res*. 1982 Jul;(167):296–302.

73. Singh P, Schwarzbauer JE. Fibronectin and stem cell differentiation - lessons from chondrogenesis. *J Cell Sci*. 2012 Aug 15;125(16):3703–12.

74. Mahsa Khatami S, Parivar K, Naderi Sohi A, et al. Acetylated hyaluronic acid effectively enhances chondrogenic differentiation of mesenchymal stem cells seeded on electrospun PCL scaffolds. *Tissue Cell*. 2020 Aug 1;65:101363.

75. Jiménez G, Venkateswaran S, López-Ruiz E, et al. A soft 3D polyacrylate hydrogel recapitulates the cartilage niche and allows growth-factor free tissue engineering of human articular cartilage. *Acta Biomater*. 2019 May;90:146–56.

76. Feng B, Ji T, Wang X, et al. Engineering cartilage tissue based on cartilage-derived extracellular matrix cECM/PCL hybrid nanofibrous scaffold. *Mater Des*. 2020 Aug 1;193:108773.

77. Caligaris M, Canal CE, Ahmad CS, et al. Investigation of the frictional response of osteoarthritic human tibiofemoral joints and the potential beneficial tribological effect of healthy synovial fluid. *Osteoarthr Cartil*. 2009 Oct;17(10):1327–32.

78. López-Ruiz E, Perán M, Cobo-Molinos J, et al. Chondrocytes extract from patients with osteoarthritis induces chondrogenesis in infrapatellar fat pad-derived stem cells. *Osteoarthr*

Cartil. 2013 Jan;21(1):246–58.

79. Perán M, Marchal J, López-Ruiz E, et al. Human cardiac tissue induces transdifferentiation of adult stem cells towards cardiomyocytes. *Cytotherapy*. 2010;12(3):332–7.

80. Mushahary D, Spittler A, Kasper C, et al. Isolation, cultivation, and characterization of human mesenchymal stem cells. Vol. 93, Cytometry Part A. Wiley-Liss Inc.; 2018. p. 19–31.

81. Baena J, Jiménez G, López-Ruiz E, et al. Volume-by-volume bioprinting of chondrocytes-alginate bioinks in high temperature thermoplastic scaffolds for cartilage regeneration. *Exp Biol Med*. 2019 Jan 10;244(1):13–21.

82. Kang H-W, Yoo JJ, Atala A. Bioprinted Scaffolds for Cartilage Tissue Engineering. In 2015. p. 161–9.

83. Akkineni AR, Ahlfeld T, Lode A, et al. A versatile method for combining different biopolymers in a core/shell fashion by 3D plotting to achieve mechanically robust constructs. *Biofabrication*. 2016 Oct 7;8(4):045001.

84. Penick KJ, Solchaga LA, Berilla JA, et al. Performance of polyoxymethylene plastic (POM) as a component of a tissue engineering bioreactor. *J Biomed Mater Res A*. 2005 Oct 1;75(1):168–74.

85. Burkhardt D, Hwa S-Y, Ghosh P. A novel microassay for the quantitation of the sulfated glycosaminoglycan content of histological sections: its application to determine the effects of Diacerhein on cartilage in an ovine model of osteoarthritis. *Osteoarthr Cartil*. 2001 Apr;9(3):238–47.

86. Donath K, Breuner G. A method for the study of undecalcified bones and teeth with attached soft tissues. The Säge-Schliff (sawing and grinding) technique. *J Oral Pathol*. 1982

Aug;11(4):318–26.

FIGURES

Figure 1

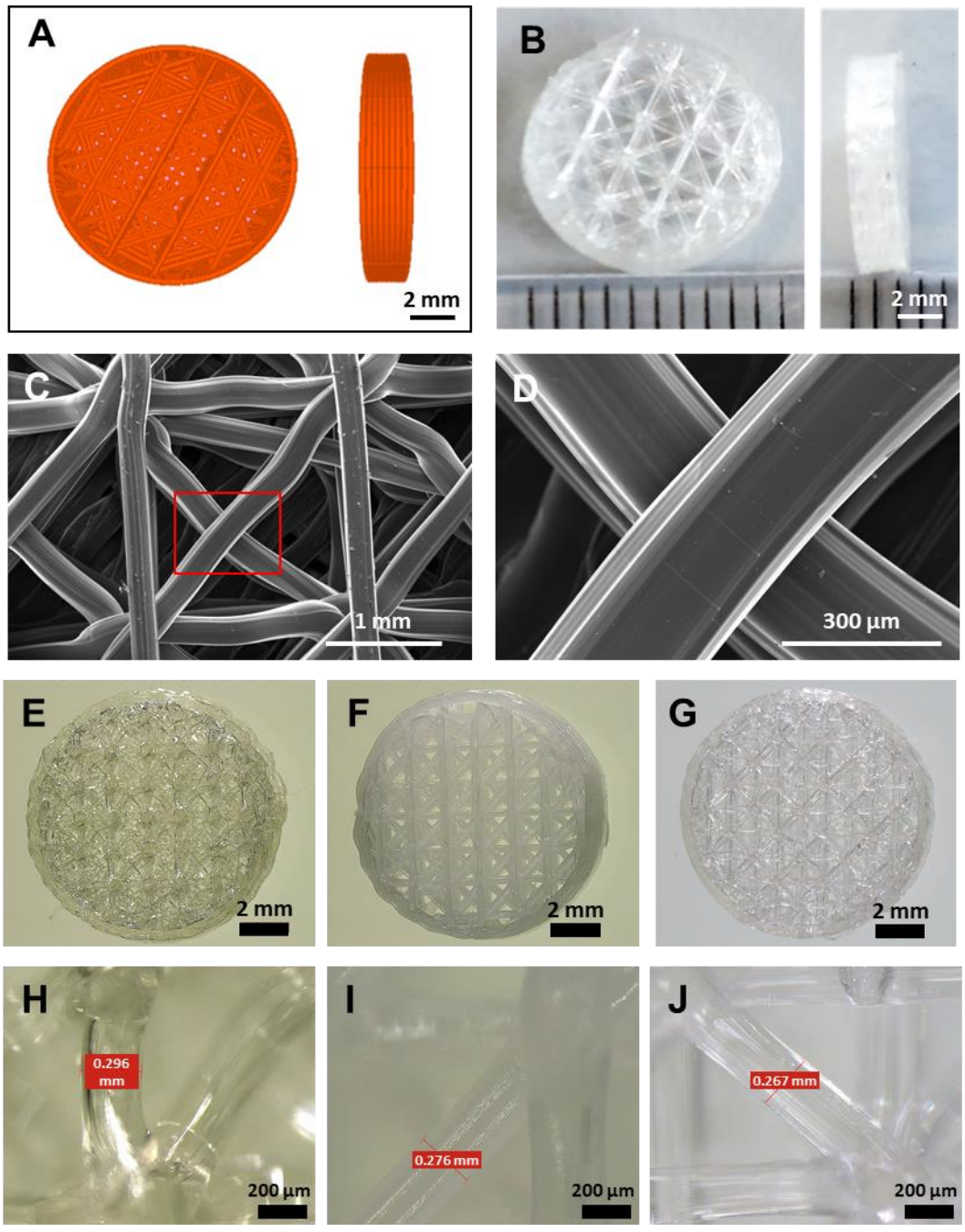

Figure 2

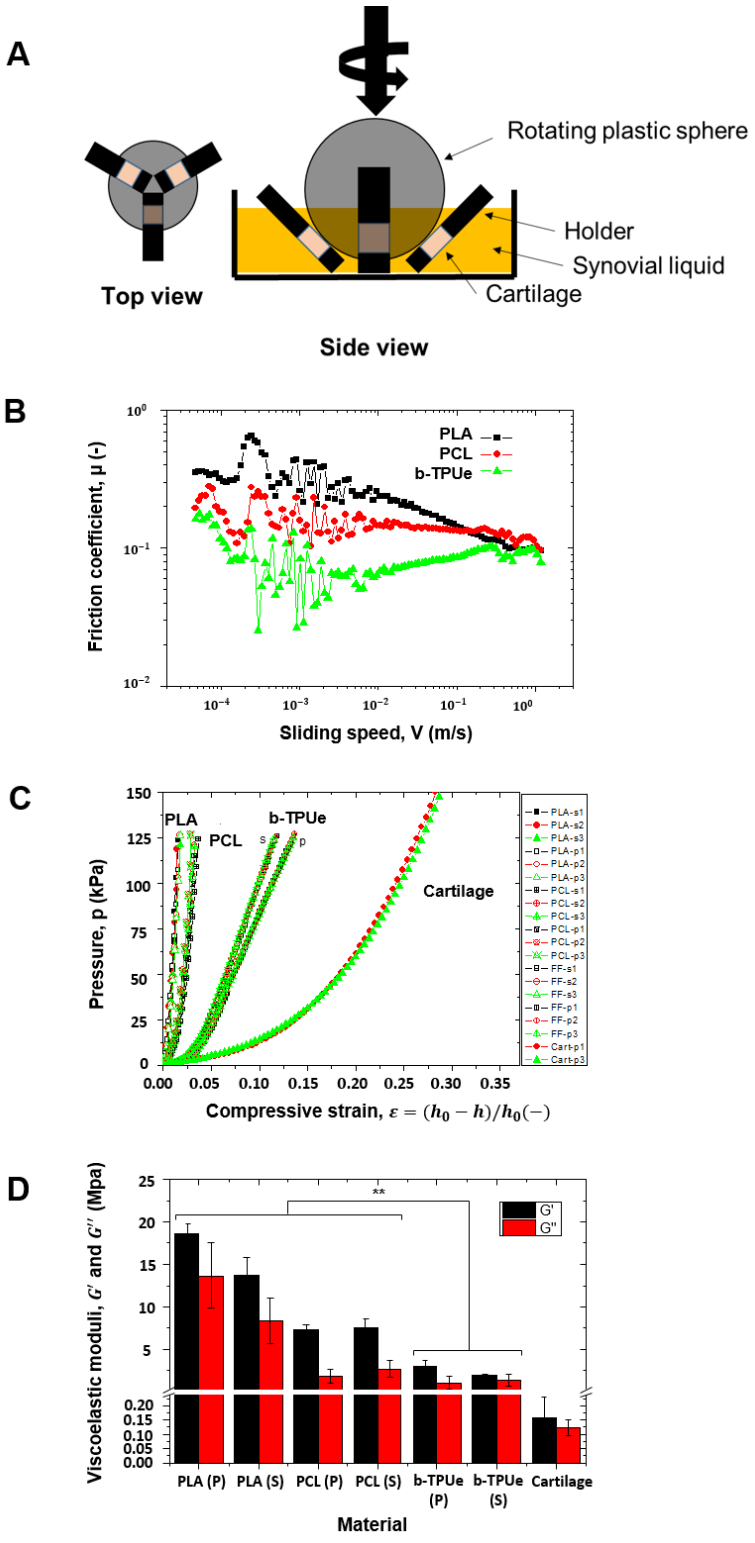
A
Rotating plastic sphere
Holder
Synovial liquid
Cartilage
Top view
Side view
B
Friction coefficient, μ (-)
PLA
PCL
b-TPUe
Sliding speed, V (m/s)
C
Pressure, p (kPa)
PLA
PCL
b-TPUe
Cartilage
Compressive strain, $\varepsilon = (h_0 - h)/h_0(-)$
D
Viscoelastic moduli, G' and G'' (Mpa)
G'
G''
**
PLA (P)
PLA (S)
PCL (P)
PCL (S)
b-TPUe (P)
b-TPUe (S)
Cartilage
Material

Figure 3

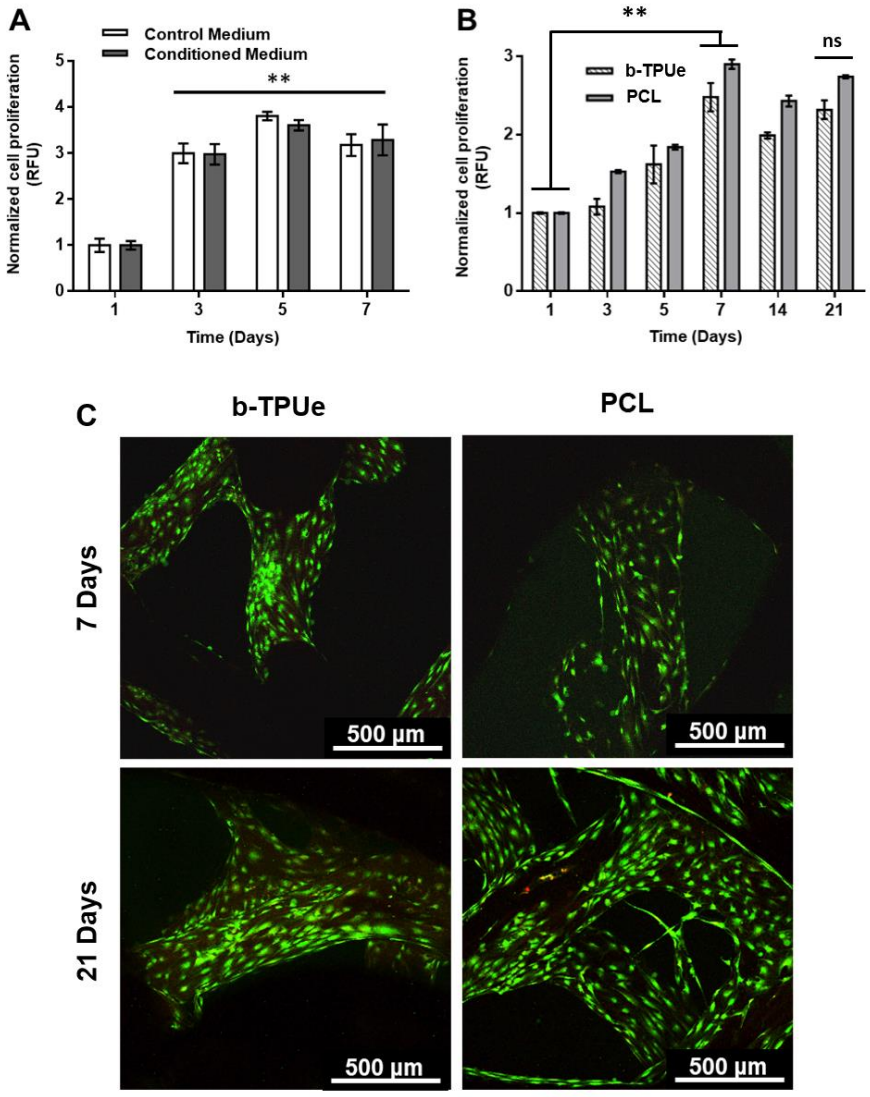
A
Control Medium
Conditioned Medium
**
Normalized cell proliferation (RFU)
Time (Days)
B
**
ns
b-TPUe
PCL
Normalized cell proliferation (RFU)
Time (Days)
C
b-TPUe
PCL
7 Days
21 Days
500 µm

Figure 4

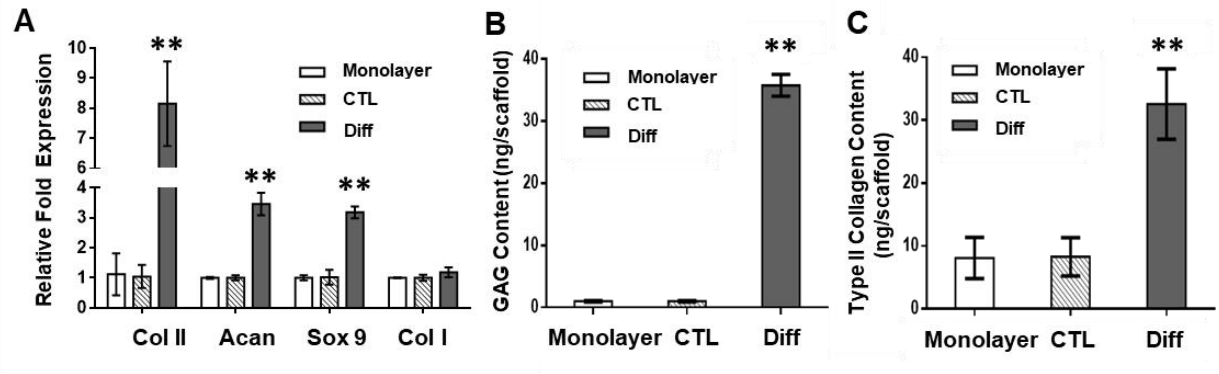
A
Relative Fold Expression
Monolayer
CTL
Diff
**
Col II
Acan
Sox 9
Col I
B
GAG Content (ng/scaffold)
Monolayer
CTL
Diff
C
Type II Collagen Content (ng/scaffold)
Monolayer
CTL
Diff

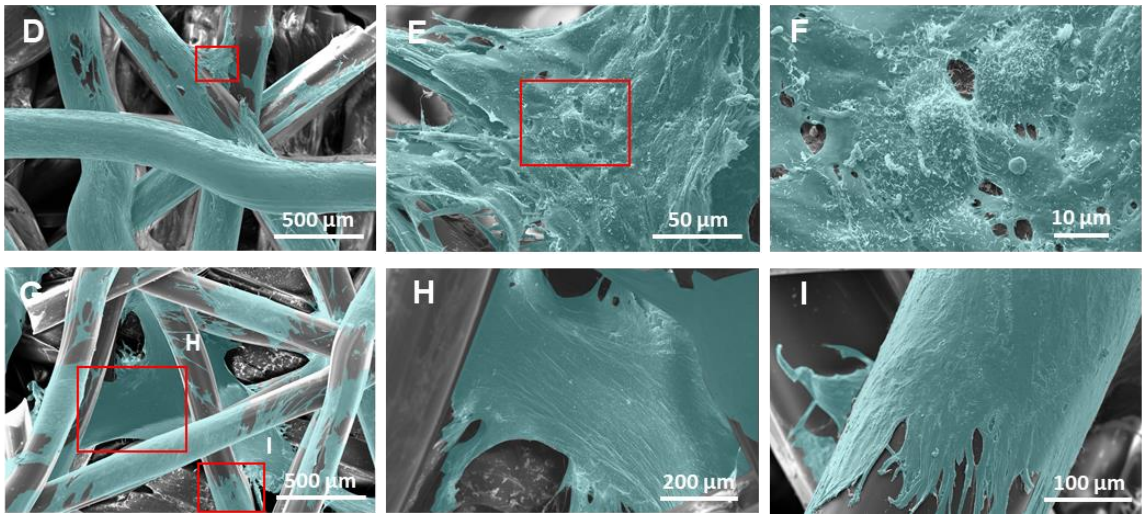
D
E
F
500 µm
50 µm
10 µm
G
H
I
500 µm
200 µm
100 µm

Figure 5

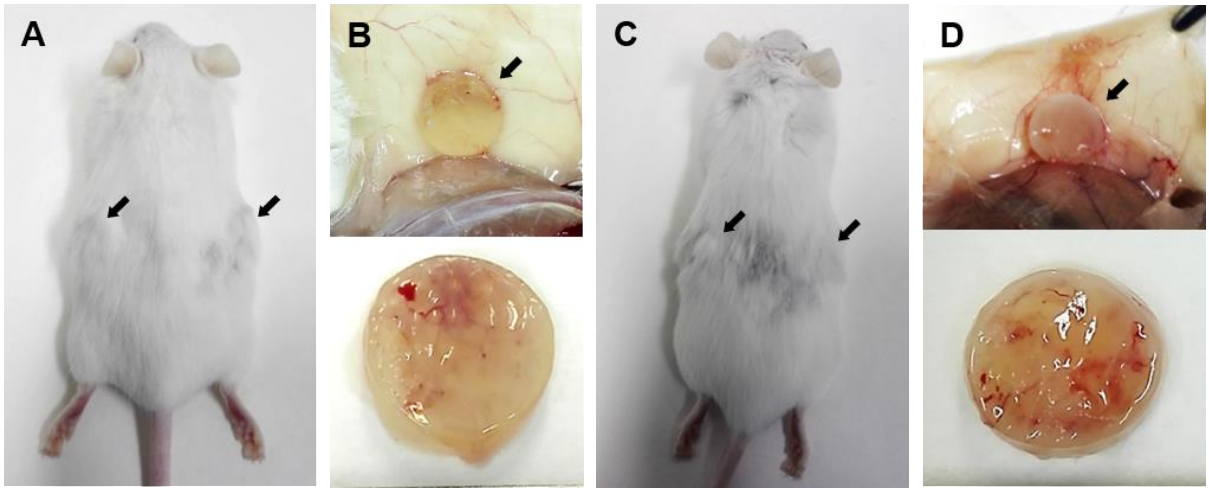

Figure 6

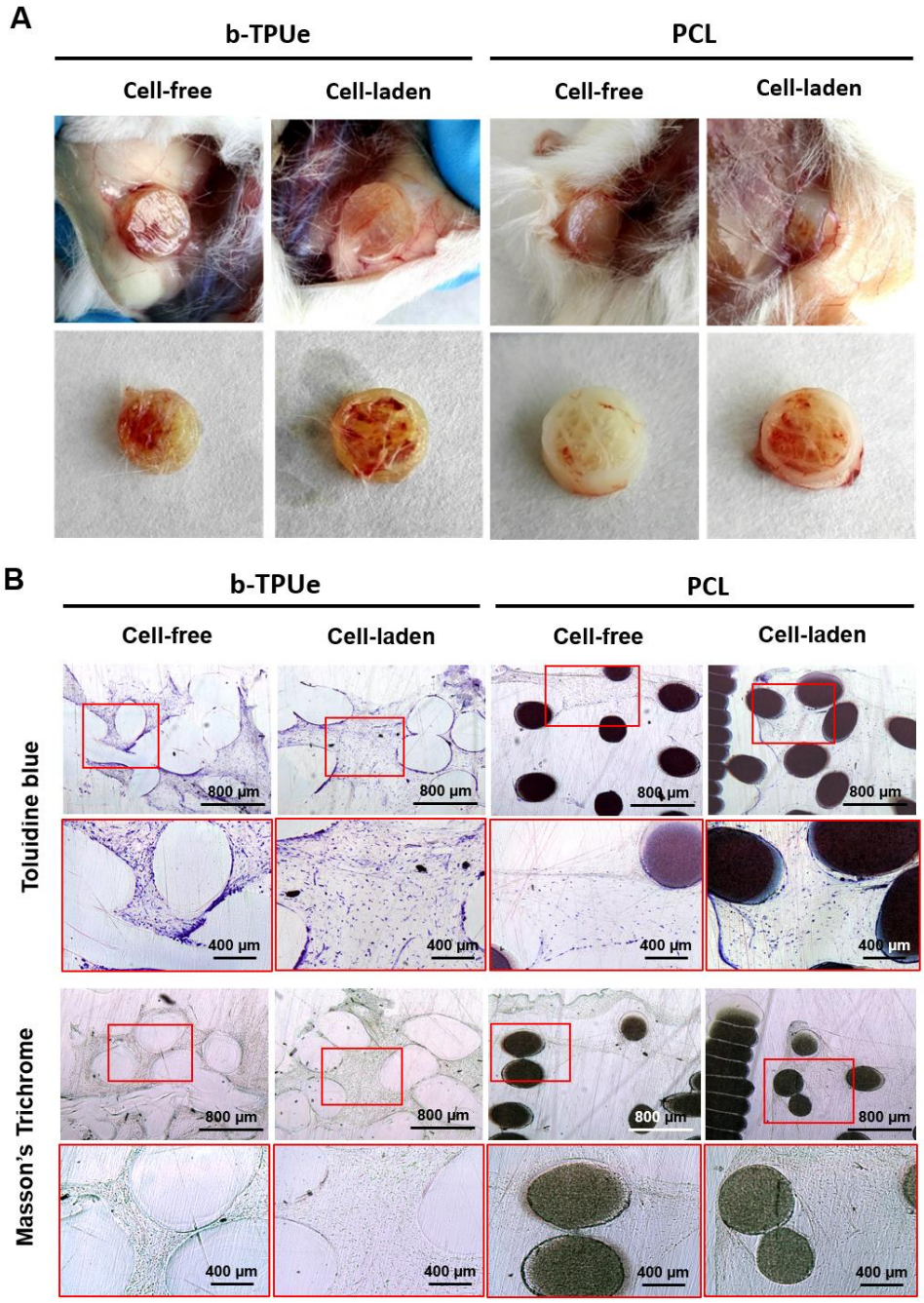
A
b-TPUe
PCL
Cell-free
Cell-laden
Cell-free
Cell-laden
B
b-TPUe
PCL
Cell-free
Cell-laden
Cell-free
Cell-laden
Toluidine blue
Masson's Trichrome
800 μm
400 μm

Table 1. Primer sequences

Gene	Forward	Reverse
Col 1	ATGGATGAGGAAACTGGCAACT	GCCATCGACAAGAACAGTGTAAGT
Col 2	GAGACAGCATGACGCCGAG	GCGGATGCTCTCAATCTGGT
Acan	AGGATGGCTTCCACCAGTGC	TGCGTAAAAGACCTCACCCTCC
Sox 9	GAGCAGACGCACATCTC	CCTGGGATTGCCCCGA
Gapdh	TGCACCACCAACTGCTTAGC	GGCATGGACTGTGGTCATGAG

Graphical table of contents

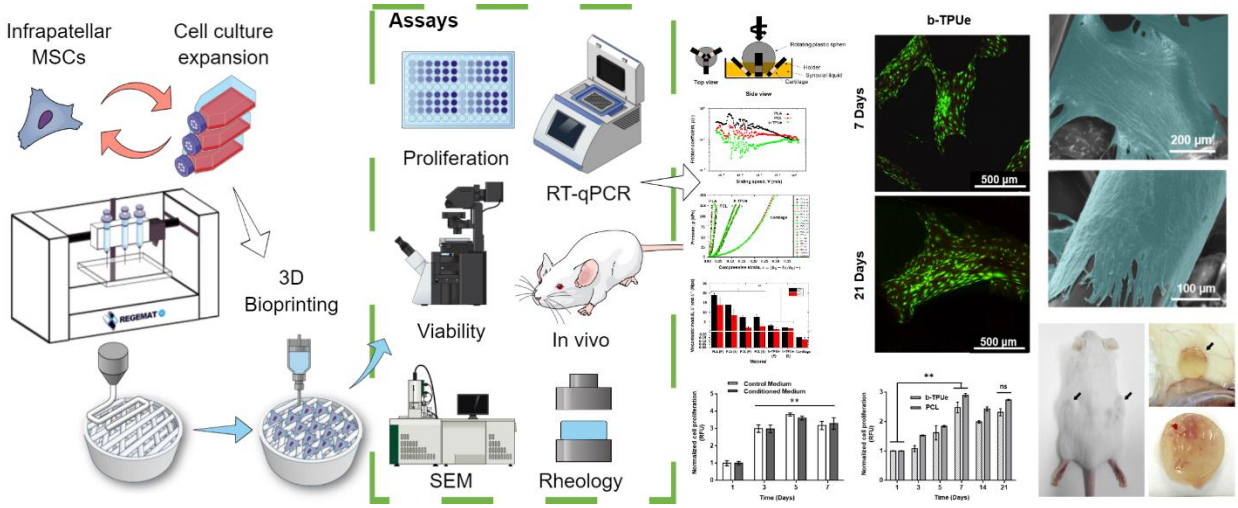

FIGURE LEGENDS

Figure 1. B-TPUe scaffolds design: (**A)** CAD model of the scaffold design. (**B)** 3D printed b-TPUe scaffold (10 mm in diameter and 3 mm in height). (**C, D)** SEM images of the top surface of b-TPUe 3D printed scaffolds (scale bars: 1 mm and 300 μm respectively). **(E-G)** Macroscopic view of b-TPUe, PCL and PLA scaffolds, respectively. **(H-J)** Scaffold fibre width of b-TPUe, PCL and PLA scaffolds, respectively.

Figure 2. Tribological and rheological characterization. (**A)** Schematic diagram of the tribological set-up. **(B)** Frictional behaviour of PLA (black), PCL (red) and b-TPUe (green). (**C)** Compression curves corresponding to the studied samples (s: solid; p: porous). (**D)** Linear viscoelastic moduli (G' and G'') for the materials studied (** = $p < 0.01$). Graphs created using the Origin 9.0 software.

Figure 3. *In vitro* biocompatibility of b-TPUe bioprinted scaffolds with MSCs. (A) Proliferative potential of MSCs cultured with control (DMEM 10% FBS, 1% P/S) or b-TPUe-conditioned medium up to 7 days (** = $p < 0.01$). **(B)** MSCs proliferation cultured in both b-TPUe and PCL bioprinted scaffolds up to 21 days with no significant differences between PCL and b-TPUe (no significance: ns). Significant cell growth was observed in both materials at day 7 of culture in both materials (** = $p < 0.01$) (RFU: Relative fluorescence units). **(C)** Representative confocal images of MSCs grown in both b-TPUe and PCL bioprinted scaffolds at day 7 and 21. Live/dead assay was employed, using calcein (green) and ethidium homodimer (red), live cells were stained green while dead cells were stained red. Scale bars: 500 μm. Graphs created using the GraphPad Prism 6.01 software.

Figure 4. MSCs chondrogenic differentiation in b-TPUe bioprinted scaffolds. Chondrogenic differentiation was evaluated in MSCs cultured in monolayer, b-TPUe scaffolds (CTL), and b-TPUe scaffolds under differentiation conditions (Diff) after 21 days in culture. **(A)** RT-PCR analysis of chondrogenic key markers. **(B)** GAGs quantification. **(C)** Type II collagen quantification. **(D-F)** SEM representative images of MSCs growing in b-TPUe bioprinted scaffolds at day 21 (** = $p < 0.01$). **(G-I)** SEM representative images of MSCs growing in b-TPUe bioprinted scaffolds under chondrogenic differentiation conditions. Scale bars: 500 µm (**D**), 50 µm (**E**), 10 µm (**F**), 500 µm (**G**), 200 µm (**H**), 100 µm (**I**). Graphs created using the GraphPad Prism 6.01 software. SEM images false-coloured using the cross-platform image editor GIMP (version 2.10.14).

Figure 5. *In vivo* biocompatibility of b-TPUe. (**A**) Macroscopic image of the locations of implanted b-TPUe scaffolds in CD1 mice. Scaffolds were implanted in the dorsal region of 8 weeks old CD1 mice and resected 21 days after surgery procedure. **(B)** Images of b-TPUe scaffolds recovered from CD1 mice. **(C)** Macroscopic image of the locations of implanted PCL scaffolds in CD1 mice. **(D)** Images of PCL scaffolds implanted in the dorsal region of CD1 mice.

Figure 6. *In vivo* biocompatibility of b-TPUe bioprinted scaffolds with MSCs. (A) Macroscopic images for cell-free and cell-laden b-TPUe and PCL scaffolds fabricated by 3D bioprinting. Scaffolds were implanted in the dorsal region of 8 weeks old female NSG mice and resected 21 days after surgery procedure. (**B)** Histologic analysis of Toluidine blue and Masson´s Trichrome staining of cell-free and cell-laden b-TPUe and PCL scaffolds 3 weeks post-implantation. Scale bars: 800 µm for black-labelled images, and 400 µm for red-labelled images.